frontiers in Energy Research

ORIGINAL RESEARCH
published: 06 April 2021
doi: 10.3389/fenrg.2021.653203

# Synergy of Oxygen Plasma and $Al_2O_3$ Atomic Layer Deposition on Improved Electrochemical Stability of Activated Carbon-Based Supercapacitor

*Fuming Zhang[1], Guanghui Song[1], Dayakar Gandla[1], Yair Ein-Eli[2]* and Daniel Q. Tan[1]**

[1] Guangdong Technion Israel Institute of Technology, Shantou, China, [2] Technion – Israel Institute of Technology, Haifa, Israel

OPEN ACCESS

**Edited by:**
Francesco Ciucci,
Hong Kong University of Science and Technology, Hong Kong

**Reviewed by:**
Huan Pang,
Yangzhou University, China
Xifei Li,
Xi'an University of Technology, China
Haitao Zhang,
Chinese Academy of Sciences, China

***Correspondence:**
Daniel Q. Tan
daniel.tan@gtiit.edu.cn
Yair Ein-Eli
eineli@technion.ac.il

**Specialty section:**
This article was submitted to Electrochemical Energy Conversion and Storage, a section of the journal Frontiers in Energy Research

**Received:** 14 January 2021
**Accepted:** 15 March 2021
**Published:** 06 April 2021

**Citation:**
Zhang F, Song G, Gandla D, Ein-Eli Y and Tan DQ (2021) Synergy of Oxygen Plasma and $Al_2O_3$ Atomic Layer Deposition on Improved Electrochemical Stability of Activated Carbon-Based Supercapacitor. Front. Energy Res. 9:653203. doi: 10.3389/fenrg.2021.653203

As a conventional electrode material of electric double-layer capacitors (EDLC), activated carbon (AC) still faces challenges to exhibit high capacitance. To address this problem, herein, we introduce a combined method of oxygen plasma and $Al_2O_3$ tomic layer deposition (ALD) on AC electrodes to reduce the impedance and improve the cycle stability of EDLC. The defect structure can be precisely designed by simply tuning the oxygen-plasma treatment time, thereby affecting the microstructures of AC electrode. Such a tactic permits the first-operated AC electrode with more defects and the ALD passivation of AC resulting in an outstanding rate performance for the device (40.6 F $g^{-1}$ at 5 mA $cm^{-2}$, 20.1 $Fg^{-1}$ at 100 mA $cm^{-2}$) and cycling stability (∼90% retention after 5,000 cycles). This benefit from the synergistic effect of defects from doped oxygen and stable aluminum oxide layer on the electrode surface. This work delivers a feasible strategy to construct a stable AC material with superior cycling performance for supercapacitor.

**Keywords: supercapacitors, high voltage, aluminum oxide, atomic layer deposition, porous activated carbon**

## INTRODUCTION

The demand of advanced energy storage system drives the search for new types of renewable energy materials and devices to reduce the environmental and pollution issues. Electrochemical supercapacitor (ES) has some obvious advantages in high power density to render a rapid charge-discharge rate (within seconds) for short-term acceleration and recovery of energy from braking, and long cycle life (>100,000 cycles) compared with battery devices. However, the lower energy density limits the broad application of supercapacitors (Simon and Gogotsi, 2008; González et al., 2016; Xue et al., 2018). Generally, some strategies are applied to improving the device specific energy such as modifying the type/ratio of solvents in electrolytes; inducing nanoscale reaction such as doping heteroatom (N, O, S, and P), defects, and nanostructure of electrode materials; synthesizing carbons with inert surface or passivation to suppress the side reaction or interaction between the electrolytes and the electrodes (Shen and Hu, 2014; Chi et al., 2016; Li et al., 2020). In principle, supercapacitor's performance highly depends on the electrodes' specific surface area, pore structure, surface functionality, and electrical conductivity (Wang et al., 2013; Li et al., 2020).

As such, activated carbon (AC) is the most widely used electrodes in electric double-layer capacitors (EDLCs), which possesses high surface area (900–3,500 $m^2\ g^{-1}$), and gravimetric capacitances of 200–550 F $g^{-1}$ in aqueous electrolyte and 130–230 F $g^{-1}$ in non-aqueous electrolyte (Murphy et al., 2006; Yan et al., 2013). However, ACs with various functional groups may accelerate the side reaction between electrolytes and electrodes leading to capacity loss, leakage current, limited working voltage window in non-aqueous electrolyte system (Yoshida et al., 1990; Morimoto et al., 1996; Pandolfo and Hollenkamp, 2006). The universal approaches to enhance energy storage capacity of AC-based supercapacitors are utilizing a hierarchical nanostructure, composite with metal oxides, conducting polymers favorable for Faradaic reaction, and properly functionalizing carbon materials for improved surface wettability (Balasubramaniam et al., 2020; Qin et al., 2020). Besides, some metal-organic framework-derived materials and Mxene-based composites are confirmed to boost the energy storage capacity as well (Liang et al., 2019; Wang et al., 2020).

Sui et al. (2015) synthesized $Ni(OH)_2$/AC/CNT composite by microwave-assisted method, displaying a specific capacitance of 82 F $g^{-1}$, energy density of 32.3 Wh $kg^{-1}$ at a power density of 504.8 W $kg^{-1}$ with 83.5% capacitance retention after 1,000 cycles in an asymmetric supercapacitor. Elmouwahidi et al. (2017) utilized an inverse emulsion method to obtain carbonxerogel-$TiO_2$ composites for symmetric supercapacitors. The device shows the high electrochemical performance with 137 F $g^{-1}$ at 0.250 A $g^{-1}$ for the composite containing 20% $TiO_2$. However, the critical drawbacks of the AC materials insulated with metal oxides are huge volume and structural changes upon cycling (Eftekhari, 2017). On the other hand, the modification of AC-based electrodes and biomass-derived carbon draw great interest for the design of wide range of pore size that could provide a larger adsorption area and thus a higher specific capacitance. The resulted AC electrode using biomass precursors such as walnut shell, seaweed, wood, starch, corn cob, rubber fiber, and coffee grounds, etc. demonstrated significant electrochemical performance (Korenblit et al., 2012; Li et al., 2019; Gandla et al., 2020). Although the development of proper pore structure in carbon material remains to be an important pathway for high specific capacitance at high power, the manufacturing of AC electrodes using the wide precursors requires low temperature pre-carbonization and activation process (Surendran et al., 2018; Liu et al., 2019; Zeng et al., 2019). The AC products carry certain amount of surface functionalities such as oxygen and OH group that can become the root cause of the performance degradation during cyclic operation. Eliminating or suppressing their reactivity with electrolytes as well as enhancing the capacity of AC-based supercapacitor are very attractive to the energy storage device.

This work reports a new approach combining plasma treatment and atomic layer deposition (ALD) coating technique to synergistically achieve the high capacitance and stable cycling performance using AC electrodes. In low-temperature plasma, the strong electromagnetic fields generates energetic electrons that can dissociate, ionize, or excite the gas molecules. As a result, a large number of gas ions, atoms, and excited species are created in the plasma treatment process (Kim et al., 2016; Tran et al., 2016). The introduction of heteroatoms is highly reactive and intensively interacts with the AC materials for electrode modification. Quan, et al. confirmed that the exfoliation and reduction of GO have been successfully achieved in DBD plasma with different working gases, including H2 (reducing), Ar (inert), and $CO_2$ (oxidizing; Zhou et al., 2012). Ouyang et al. (2016) considered that the high activity of $N_2$ plasma can also be active enough to dope into carbon materials. However, this method may also introduce heteroatoms like defects and vacancies into carbon materials (Tao et al., 2016; Zhang et al., 2017).

Different from plasma, ALD has been demonstrated capable for effective oxide coating on various cathode materials for lithium ion batteries and enabling three-dimensional-structure materials for the enhanced cycling performance at higher voltages (Chen et al., 2010; Liu et al., 2012; Jung et al., 2013; Gandla and Tan, 2019). In this work, the author attempted to leverage ALD technique to modify the conventional AC electrode (not powder) that holds the interior carbon structure through oxygen plasma treatment. The subsequent deposition of nanometer-thick $Al_2O_3$ is anticipated to stabilize the AC electrode from the reactive degradation of the functional groups. The high electrochemical capacity of plasma-enhanced AC electrodes may synergize with the high cycling retention of ALD oxide protection, thus giving rise to higher energy density and power density.

# EXPERIMENTAL AND SAMPLES

## Materials

Activated carbon powders were YP-50F from Kuraray, and the binder polyvinylidene difluoride (PVDF), N-methyl-2-pyrrolidinone (NMP), and carbon black super Li were purchased from (Sigma Aldrich). A 35-μm thick cellulose NKK TF4035 (Nippon Kodoshi, Japan), having 75% porosity was used as a separator. The electrolyte salt (SBP-$BF_4$) obtained from (Sigma Aldrich) was placed in a glove box filled with high purity argon (<1 ppm $O_2$ and <1 ppm $H_2O$), then dissolved in the Acetone Nitril (AN) with 1 moL/L concentrations.

## Synthesis of Oxygen Plasma Treated ACs

Oxygen Plasma Etching on ACs: The carbon electrode was prepared by mixing 85% AC (Kuraray YP-50), 10% carbon black (Super Li), and 5% binder of PVDF. Then a vaccum mixer was used for 10 min to achieve a homogeneously mixed carbon slurry by adding solution NMP. The slurry was coated on an aluminum foil collector and dried in a vacuum oven overnight at 120°C. The oxygen-plasma-treatment of the ACs electrodes were carried out as shown in **Figure 1** with reactive ion etching power (40 W), plasma pressure (90 Pa), $O_2$ flow rate (700 mL $min^{-1}$), and operated time of 5, 15, and 30 min, respectively. The resulted material was named as OPx ($x$ = 5, 15, and 30). Finally, the treated electrode was pressed to a dense sheet at 10 MPa to obtain the working electrodes. The punched circular disks with a diameter of 12 mm were obtained as electrode using MTI disk cutting machine (MSK-T10). The loaded active mass on each working electrode was about 2.2–2.4 mg $cm^{-2}$.

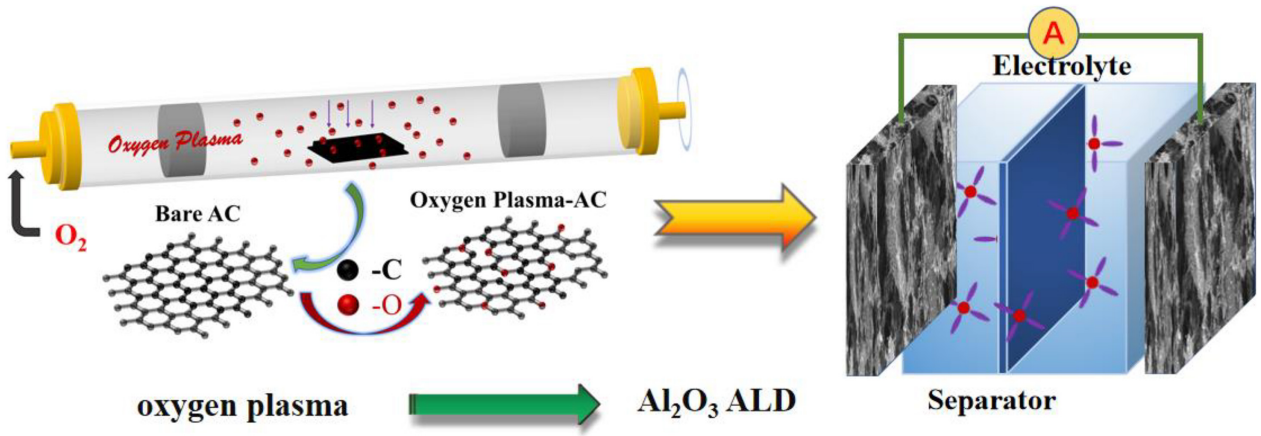


**FIGURE 1 |** Illustration for the function of oxygen plasma, $Al_2O_3$ ALD coating on the AC electrode, and the construction of AC-based symmetric supercapacitor.

## Synthesis of ALD Oxide Coated ACs

Atomic layer deposition coating was carried out using a Benchtop GESTar XT-D ALD system by Arradiance, Inc. Aluminum oxide ($Al_2O_3$) is deposited using the Trimethyl Aluminum (TMA), and high-performance liquid chromatography grade $H_2O$ (HPLC, Sigma-Aldrich). The typical growth rate for the chemistry is 0.5–1.5 Å per cycle for dielectric oxide materials. The reaction sequence within each deposition cycle was: (i) exposure of the substrate to TMA, (ii) purge to remove the nonreacted precursors and the byproducts, (iii) exposure of the substrate to $H_2O$, and (iv) purge to remove the nonreacted precursors and the byproducts (Zhao and Wang, 2013; Song and Tan, 2020).

The oxygen-plasma-treated AC electrodes were fixed onto a silicon wafer with Kapton tapes. Each ALD process was conducted in the 150°C chamber and at the constant argon flow rate of 10 sccm. The $Al_2O_3$ ALD coated electrodes were transferred into clean zip-lock storage bags or used for electrochemical tests immediately after the deposition.

## Characterization of Electrodes

The surface morphology and particle size were characterized using a ZEISS Sigma-500 field emission scanning electron microscopy. The elemental distribution and mapping were obtained using Energy Dispersive Spectroscopy (EDS, BRUKE XFlash-6130, Germany). Transmission electron microscopy (TEM) images were captured on a JEM2100 instrument at an acceleration voltage of 200 kV, to analyze the features of deposition on the carbon surface. Quantachrome Autosorb-iQ2-MP (United States) and nitrogen isotherms were used to test specific surface areas by BET tests with degassing at 250°C for 3 h for each 36 mg sample. The element distribution and functional changes were explored using X-ray photoelectron spectroscopy of Thermo Scientific ESCALAB 250Xi (United States) and monochromatic Al target.

## Electrochemical Measurements

The supercapacitor's performance of the AC, OPx, and ALD coated AC electrodes was evaluated by assembling a symmetrical supercapacitor device in a CR2032 coin using the Gamry electrochemical workstation (Interface 1010E, United States) and Arbin Station (Arbin System, United States). The Galvanostatic charge-discharge (GCD) measurement is carried out between 5 and 100 mA $cm^{-2}$. EIS data were recorded with a potential amplitude of 5 mV within a frequency range of 10–0.01 Hz (Yan et al., 2020).

The specific capacitance ($C$, F $g^{-1}$), energy density ($E$, Wh $kg^{-1}$), and coulombic efficiency ($\eta$) values of the coin cell supercapacitor device were calculated using GCD curves from the following equations:

$$C = \frac{I\Delta t}{m\Delta V} \tag{1}$$

$$\eta = \frac{\Delta td}{\Delta tc} \tag{2}$$

$$E = \frac{C\Delta V^2}{2 \times 3.6} \tag{3}$$

where $I$ represents the discharge current (A), $\Delta t$ is the discharge time (s), $m$ is the total mass (g) of active material loaded on both the electrodes, $\Delta V$ denotes the applied potential window (V), and $\Delta td/\Delta tc$ is the ratio of discharge time to charge time.

# RESULTS AND DISCUSSION

## Microstructural Analysis of Oxygen-Plasma-Treated Electrode

**Figure 2** shows the surface microstructure of the bare AC electrode and the AC treated with different oxygen-plasma-treated time. Compared with the bare AC, the surface structure of AC via plasma treatment was gradually damaged and roughened up with increasing treatment time. Apparently, the AC structure could no longer maintain the intact block structure after 30 min. This may be attributed to destruction of the original C-C bonds under plasma energy and the formation of new functional group bonds and defective structures.

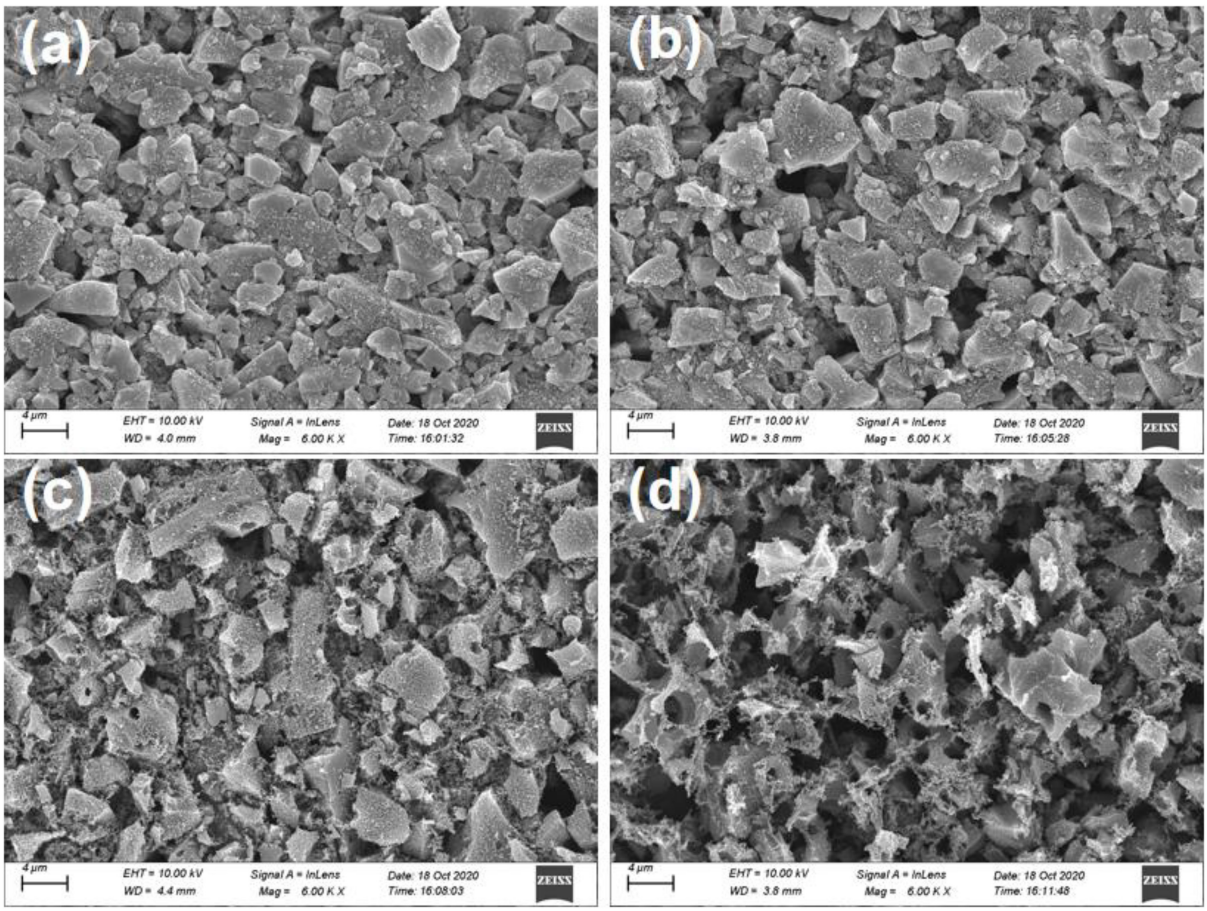


**FIGURE 2 |** SEM image:**(a)** Bare AC; **(b)** Oxygen-Plasma treatment at 5 min (OP-5); **(c)** Oxygen-Plasma treatment at 15 min (OP-15); and **(d)** Oxygen-Plasma treatment at 30 min (OP-30).

The molecular structure of the damaged AC samples was further inspected using Raman spectroscopy. All the samples exhibit similar Raman lines with two of them relatively dispersed near ∼1,350 $cm^{-1}$ (D band) and ∼1,580 $cm^{-1}$ (G band), as shown in **Figure 3A**. With the increase in the oxygen-plasma-treated time, the ratio of integral area of G band and D band decreases gradually. The graphitization degree of OP-x samples decreased with the increase of treated time, which indicated that the introduced oxygen relatively enhances the defect amount. The ID/IG ratios of four samples slightly increased with the increase of treated time, illustrating the increased defects as well (Tao et al., 2016).

In order to understand whether oxygen plasma treatment blocks micropores, we carried out the pore structure analysis (or pore size distribution) of plasma treated ACs and the bare AC. **Figure 3B** shows the comparison using DFT (density functional theory) and HK (Horvath-Kawazoe) methods from $N_2$ adsorption-desorption isotherms (at 77.4 K). The BET specific surface area, pore volume of the bare AC, OP-5, OP-15, and OP-30 were found to be 1,375 $m^2\ g^{-1}$, 0.65 $cm^3\ g^{-1}$, 1,378 $m^2\ g^{-1}$, 0.65 $cm^3\ g^{-1}$, 1,423 $m^2\ g^{-1}$, 0.67 $cm^3\ g^{-1}$, and 1,368 $m^2\ g^{-1}$, 0.63 $cm^3\ g^{-1}$, respectively. The 3.2% increase in the pore volume for OP-15 and negligible difference for OP-5 and OP-30 implies that the plasma did not change the surface area and pore volume significantly.

X-ray photoelectron spectroscopy (XPS) was used to reveal the impact of oxygen insertion on the AC surface, as shown in **Figures 3C,D**. The O1s peak in the spectrum was deconvoluted into three peaks of C = O (531.5ev), C-O (532.6ev), and O-C = O (533.7ev), respectively. Compared to the bare AC electrode, the plasma treated electrodes contain more COOH groups and less O-C = O groups as the treated time extends from 5 to 30 min. The contribution of oxygen insertion and more COOH groups are favorable for improving the performance (Lai and Lo, 2015). In addition, the oxygen content increases first and then decreases as the oxygen treatment time increases. The OP-15 possess the highest oxygen content of 30.68%. The less oxygen content in electrodes with longer time plasma treatment may be resulted from the broken functional bond that damages the carbon structure and even carbon flake-off.

**Figure 4** depicts an oxygen doping effect by the Nyquist plot of impedance/frequency behavior of the bare AC based and the plasma-treated electrodes. The coin cells using plasma-treated AC shows obvious reduction in the impedance compared

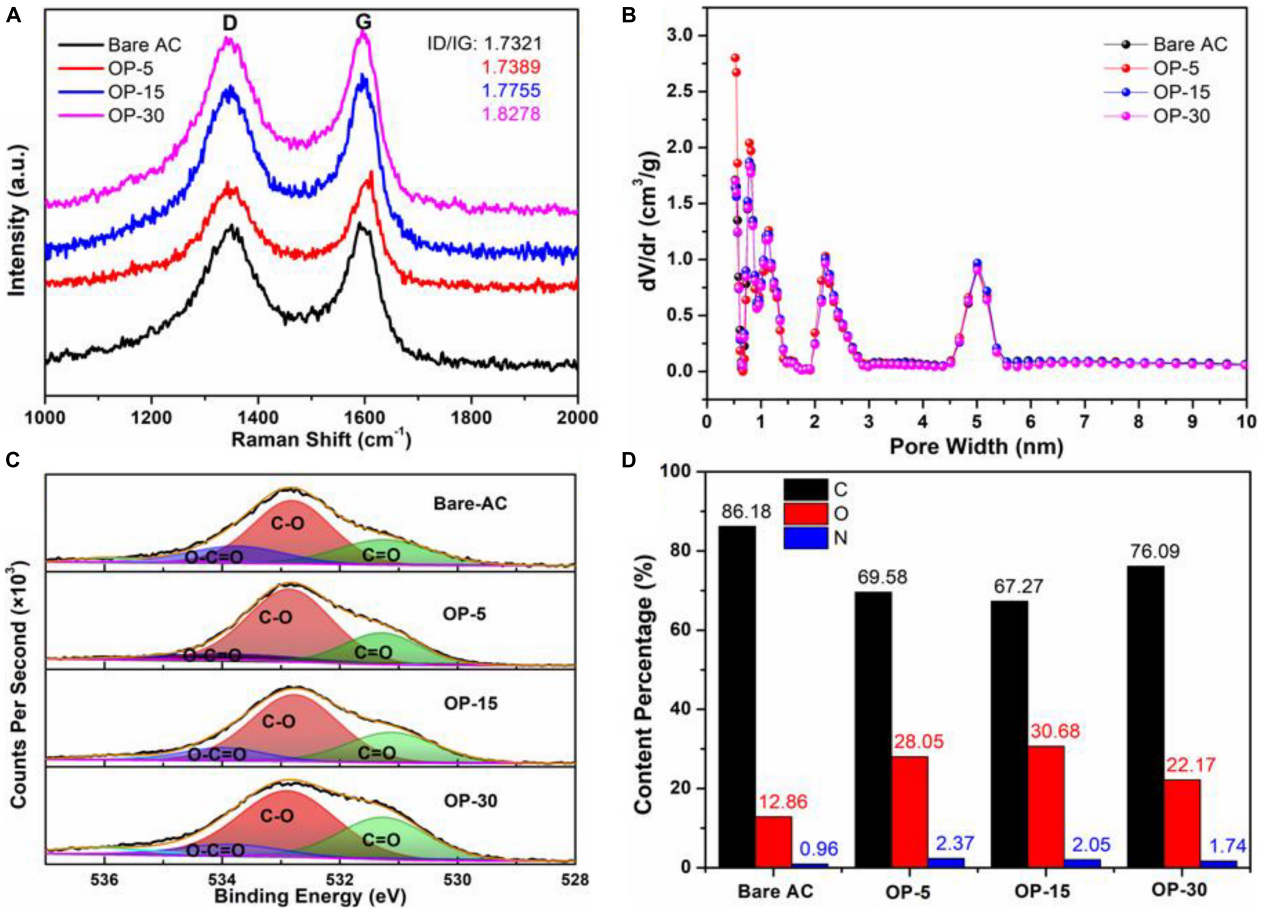


**FIGURE 3 | (A)** Raman spectra of Bare AC and OP-x; **(B)** the pore size distribution of Bare AC and OP-x; **(C)** Convolution peak of O1s spectra of Bare AC and OP-x; and **(D)** Element content percentage of Bare AC and OP-x.

with that of the bare AC. The equivalent circuit model for further analysis of the impedance data is shown as inset of **Figure 4A**. The charge-transfer resistance (Rct) values of the bare AC, OP-5, OP-15, and OP-30 were found to be 17.5, 6.72, 6.62, and 6.98 **Ω**, respectively. The equivalent series resistance ($R_s$) values were 1.5, 0.945, 0.851, and 0.825 **Ω**, respectively. Both Rct and Rs of the cells with oxygen-plasma-treated AC electrodes has a considerably lower value. It is certain that the plasma induced oxygen doping created more defects and more adequate active sites for ion adsorption. In addition, the plasma treated AC electrode becomes better wettability, which all lead to the reduced resistance behavior. Comparing with samples with different plasma treatment time, the 15-min sample (OP-15) exhibits the highest C-V loop area. The charge-discharge behaviors for the four types of electrodes as shown in **Figure 4B** exhibit the symmetrical triangular shapes. The linear voltage-time relationship indicates the reversible charge-discharge characteristics and the typical charge-discharge behavior of a double electric charge layer. Compared with the bare AC, the OP-15 electrode possesses longer discharge time than other plasma treated samples, implying that more or less the plasma treatment may not be at its ideal condition and higher capacitance requires longer time. Meanwhile, the IR-Drop in the figure presents the lower IR-Drop value for OP-15 than the counterparts in other samples, indicating the weak polarization for OP-15 sample.

**Figures 4C,D** shows the C-V curves from 5 to 100 mV $s^{-1}$ with nearly rectangular shape when using different test instrument (Arbin and Gamry), indicating the good capacitive behavior. Gamry's testing method makes up the error caused by sensitivity and setting parameters, however, the curve shapes are very similar. Besides, CV curves at 25 mV $s^{-1}$ of different samples in **Figure 4E** show the near-rectangular features. Among them, OP-15 sample presents the biggest area, indicating the optimal energy storage behavior. The cycling life performance of different samples was presented in **Figure 4F**. Among them, OP-15 has shown the higher capacitance retention before 1,000 cycles whereas slowly drops subsequently when tested at 3.2 V. The AC electrode, however, possess a stable retention behavior despite a lower capacitance. The unstable cycle life for the oxygen-plasma-treated electrodes may be associated with the inappropriate amount of oxygen functional group. A large number of highly active oxygen-containing functional groups could interact with

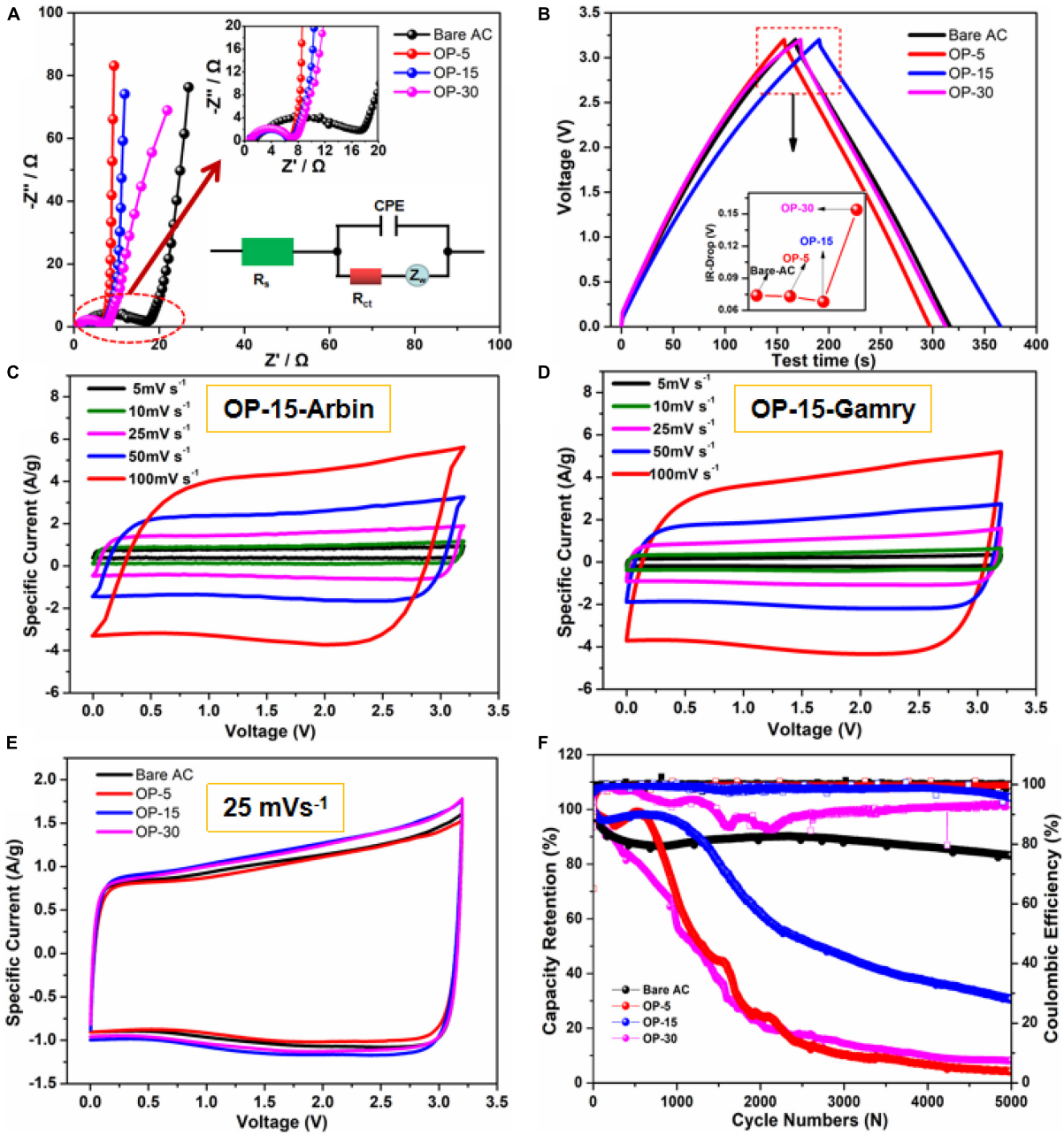


**FIGURE 4 | (A)** Electrochemical impedance spectra of Bare AC and OP-x; **(B)** A comparison GCD curves at 5 mA $cm^{-2}$ of Bare AC and OP-x (the inset shows their IR-drop curves t); **(C)** C-V curves of OP-15 using Arbin; **(D)** C-V curves of OP-15 using Gamry; **(E)** C-V curves at 25 mV $s^{-1}$ of Bare AC and OP-x; and **(F)** Cycling stability of Bare AC and OP-x at 3.2 V.

organic electrolyte after the prolonged exposure (Ju et al., 2020), which ought to be improved.

## $Al_2O_3$ ALD Improvement on Plasma-Treated Electrodes

Previous work on ALD coating on carbon surface demonstrated the improvement in lengthening cycle life (Tan et al., 2020). Herein, we further applied 20-cycle $Al_2O_3$ ALD onto the plasma treated AC electrode (OP-15) using the optimized condition for $Al_2O_3$. Basically, we investigated the sequential effect of ALD and plasma treatment on the AC electrodes: plasma treatment followed by ALD (OP15-ALD) and ALD followed by plasma treatment (ALD-OP15). With the helpful of additional deposition layer on the AC electrode, large ions can still be adsorbed into the carbon surface accordingly. **Figure 5A** shows the XPS results where the oxygen functional groups (O-C = O and C = O) in the plasma treated AC were

both apparently suppressed after ALD coating. In addition, the enhanced oxygen content are well indicative of the effective $Al_2O_3$ ALD coating regardless of the sequence of ALD and plasma treatment (**Figure 5B**).

According to the former investigation of XPS peak intensity, the improved cell cycling retention was related to the suppression of oxygen functional groups by $Al_2O_3$ coating (Zhao and Wang, 2012). Now, the presence of enhanced oxygen in both cases is indicative of a different mechanism in this work. We believe that the additional oxide layer on the carbon surface broadens the diffuse layer ($d_{Stern} + d_{coating}$) and thus renders a resistance to cycling voltage stress or a higher voltage.

To explore the details of ALD oxide coatings, TEM images were taken to detect its nanometer layer morphology on the surface of carbon. Compared with the bare AC and OP-15 electrode (**Figures 6a,b**), the aluminum oxide around 2 nm layer can be observed on the carbon surface, as shown in **Figures 6c,d**. After retention test of 5,000 cycles, the four cell samples were dissected for further inspection of the degradation. The relative intact thin layer still maintained well

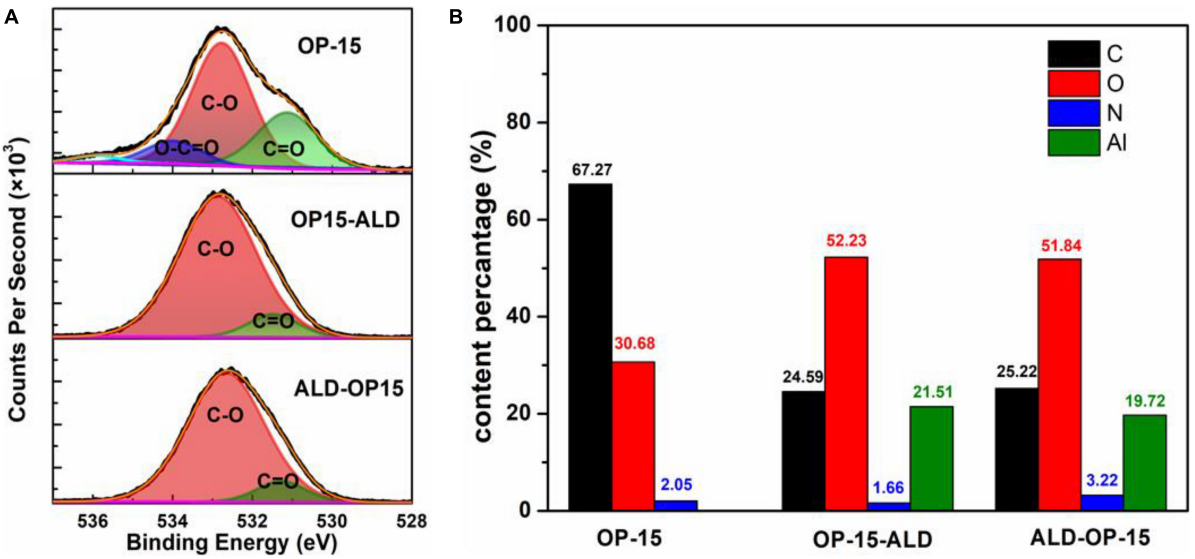


**FIGURE 5 | (A)** Convolution peak of O1s spectra of OP-15, OP15-ALD, and ALD-OP15. **(B)** Element content percentage of OP-15, OP15-ALD, and ALD-OP15.

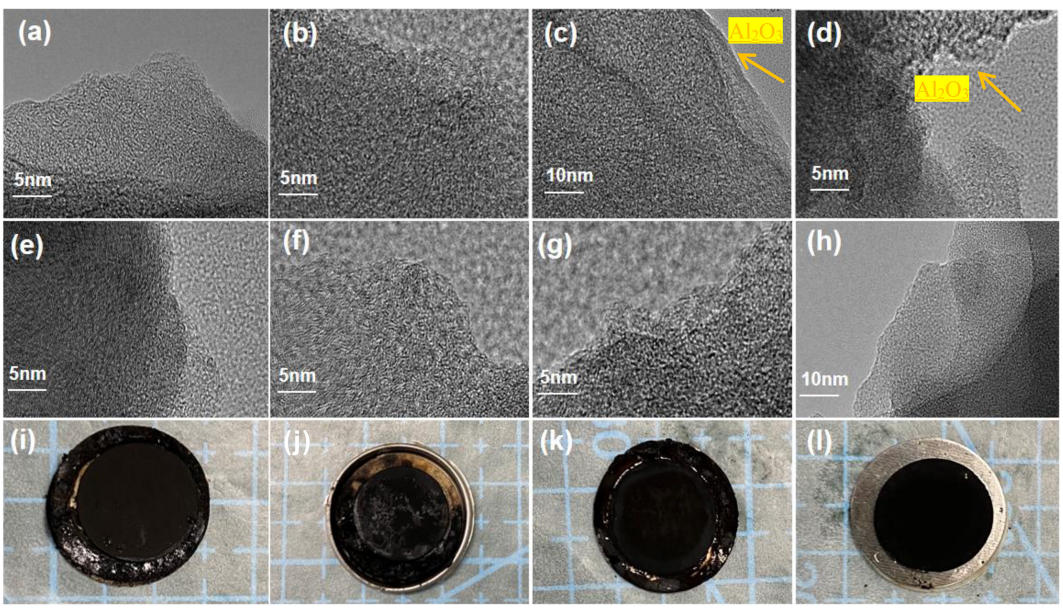


**FIGURE 6 |** TEM image of fresh electrode: **(a)** Bare AC; **(b)** OP-15; **(c)** ALD-OP15; **(d)** OP15-ALD; TEM image of electrodes after 5,000 cycles: **(e)** Bare AC; **(f)** OP-15; **(g)** ALD-OP15; **(h)** OP15-ALD; and **(i–l)** optical images of four electrodes after the cell dissection.

for the ALD-OP15 and OP15-ALD electrodes (**Figures 6e–g**). The ALD coating samples remain bright and clear. The electrodes that received plasma treatment plus ALD shows the negligible surface alteration (**Figure 6h**). On the contrary, the other three samples treated with ALD plus plasma evidently show the damages on the carbon surface, as shown by the ALD-OP15, the bare AC, and OP-15 (**Figures 6i–k**).

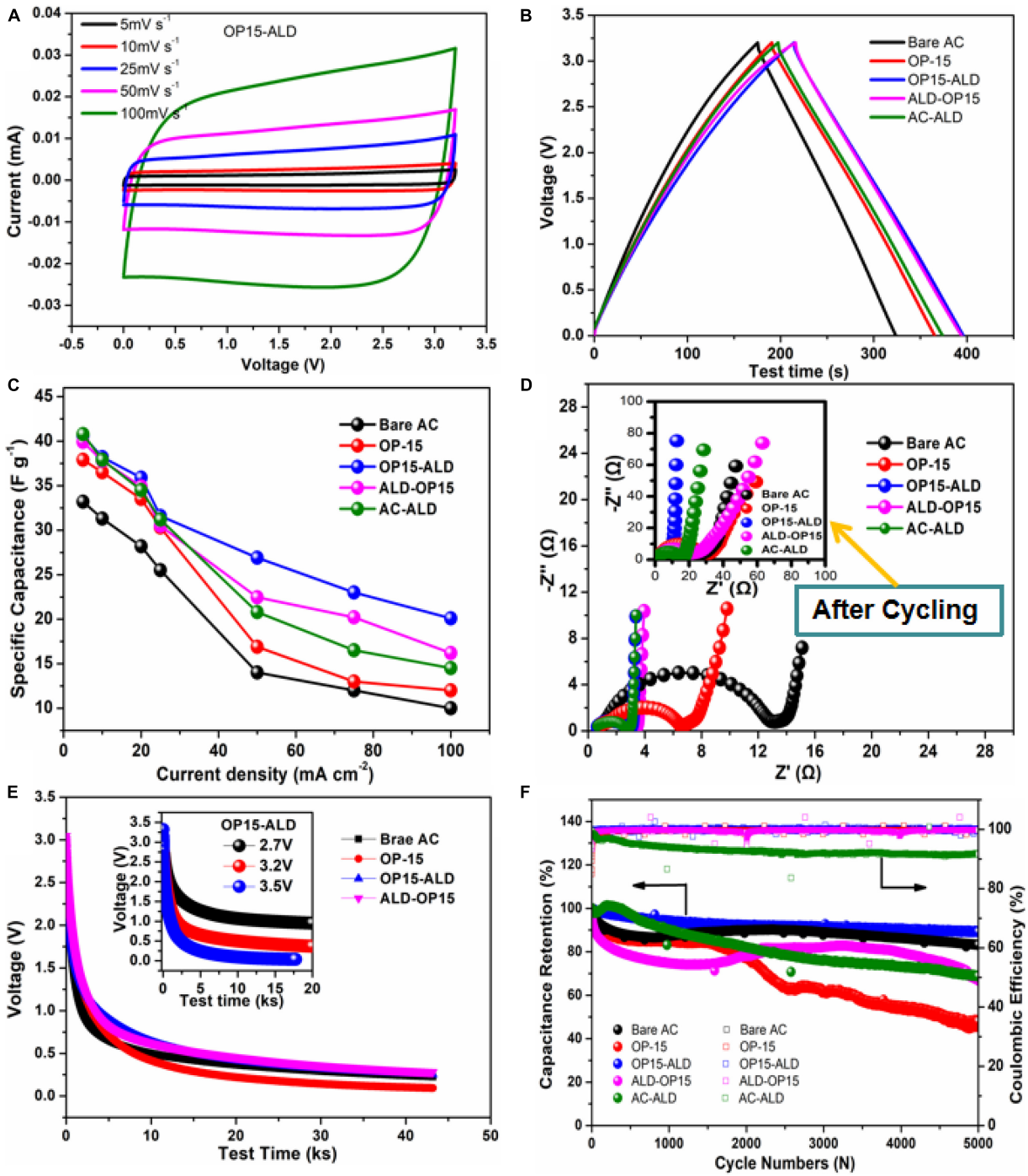


**FIGURE 7 | (A)** CV curves of OP15-ALD; **(B)** A comparison GCD curves at 5 mA $cm^{-2}$ of OP-15, OP15-ALD, ALD-OP15, and AC-ALD; **(C)** Rate capacitance of OP-15, OP15-ALD, and ALD-OP15; **(D)** Electrochemical impedance spectrum of Bare AC and OP-x (insert is the EIS after 5,000 cycles); **(E)** Self-discharge behavior (insert is OP15-ALD self-discharge after charging at 2.7, 3.2, and 3.5 V); and **(F)** Cyclic retention (solid circles) and Columbic efficiency (open circles) of 4 different electrodes.

The electrochemical performance of the ALD coating and plasma-treated AC electrodes were measured in a symmetric supercapacitor in 1 mol/L $SBPBF_4$/AN electrolyte at 3.2 V. AC electrode that has only undergone ALD treatment (AC-ALD) as a reference for the synergy of plasma and ALD. **Figure 7A** shows the CV curves of supercapacitor with OP15-ALD sample at different scanning rates. The CV curves maintained a good nearly rectangular shape at all scanning rates, and no significant distortion occurring even at a high scanning rate of 100 mV $s^{-1}$, showing the excellent capacitive characteristics and typical double-layer trait. **Figure 7B** is the GCD curve of the supercapacitor using AC electrodes with the plasma-treatment only and plasma plus ALD coating. The GCD curves show the typical triangular shape and good linearity and symmetry, indicating the good charge and discharge reversibility and the typical double-layer characteristics. Compared to the influence of different technique, the OP15-ALD and ALD-OP15 both exhibits longer discharge time than AC electrode only undergoing ALD or Plasma, indicating the higher ability of capacitance storage for the electrode with combined technique. The rate performance obtained from GCD tests of five samples are shown in **Figure 7C**.

The ALD treated electrode presents a superior rate performance compared with those of the plasma-only treated AC. Especially, the positive effect of $Al_2O_3$ coating becomes gradually apparent under higher rates. The results manifest that the additional deposition layer on the carbon surface does not generate the burden of increasing ion transport to the original material, but to improve the kinetics at high rate. We further test the impedance of the bare AC, OP-15, OP15-ALD, ALD-OP15, and AC-ALD samples with and without retention. The EIS of the samples with ALD coating evidently show lower impedance than those of the OP-15 and bare AC (**Figure 7D**). The nanometer layer deposition on the plasma-treated electrode significantly decreases the charge transfer impedance favorable for the faster ionic dynamic. Meanwhile, the impedance of OP15-ALD after 5,000 cycles is also lower than that of other counterparts. The results show that the long-term cycling almost does not influence the impedance due to the presence of $Al_2O_3$ coating layer. The lower resistance implies the reduced ion diffusion pathway that facilitates a faster ion transport between the electrolyte and surface of the electrode.

Leakage current is one of the most significant technical issues of commercial supercapacitors. This issue was also investigated on the bare AC, OP-15, OP15-ALD, and ALD-OP15 by the self-discharge test. As observed from **Figure 7E**, the open circuit potentials of the samples were measured for 12 h after charging them at a constant voltage of 3.2 V for 1 h. The OP-15 sample was maintained just 7% of its initial potential, whereas the bare AC, OP15-ALD, and ALD-OP15 maintained 14, 24, and 22% of their initial potentials, respectively. The self-discharge of OP-15 is more serious than the ALD based samples, indicating the introduction of surface functional groups would lead to greater self-discharge, while the ALD coating effectively remits the disadvantage. In addition, some reports illustrated that higher voltage level results in faster open circuit voltage decay (Kaus et al., 2010). The impact of working voltage on open circuit voltage decay is shown by the insert curve in **Figure 7E**. The sharp potential decay occurs at 3.5 V. Therefore, it is rational to choose 3.2 V as the operation voltage in the work. The ALD improvement once again proves the effectiveness of ALD oxide coating on stabilizing AC electrode stability. The retention performance of the AC electrodes of bare AC, AC-ALD, OP-15, and OP-15 with $Al_2O_3$ coating were also evaluated on the coin cell level using the same organic electrolyte. **Figure 7F** shows that the cyclic retention for the three types of coatings becomes better than those of the reference samples without ALD coating. It evidently demonstrates the effectiveness of ALD coating after the oxygen-plasma-treatment in improving the capacitance retention of AC-based EDLCs.

## CONCLUSION

This work unconventionally introduced the additional oxygen into the AC electrode by plasma treatment to increase the active sites and defects. This oxygen doping decreased the charge transfer resistance and increased the kinetics good for higher capacitance and ion transport. The capacitance retention from the plasma treatment, however, only stabilizes until 1,000 cycles. For a better retention life, the $Al_2O_3$ ALD coating demonstrated the increasing role of the cycling performance at 3.2 V. The plasma treated AC electrodes along with 2 nm thick $Al_2O_3$ effectively stabilized the capacitance retention at >90% after 5,000 cycles (>6% higher than uncoated AC electrodes, >30% higher than plasma treated AC electrodes). The nanometer oxides deposition on oxygen-contained AC electrode appears to effectively increases the C-O functional group but suppresses the C = O and O-C = O group, which reduce the activity and reactivity during the long-term cycling. The thinner ALD coating also reduced the electrical impedance more effectively than the uncoated materials. The combined role of plasma treatment and ALD coating enables the supercapacitor with stable cycling performance for conventional AC electrode.

## DATA AVAILABILITY STATEMENT

The original contributions presented in the study are included in the article/supplementary material, further inquiries can be directed to the corresponding author/s.

## AUTHOR CONTRIBUTIONS

The manuscript was written through the contributions of all authors. All authors have approved the final version of the manuscript.

## FUNDING

This research was supported by the 2020 China-Israel Special Research Grant 200902154890781.

## ACKNOWLEDGMENTS

The authors acknowledge the support of the Guangdong Technion Startup fund.

## REFERENCES


Balasubramaniam, S., Mohanty, A., Balasingam, S. K., Sang, J. K., and Ramadoss, A. (2020). Comprehensive insight into the mechanism, material selection and performance evaluation of supercapacitors. *Nano Micro Lett.* 1, 1–46. doi: 10.1007/s40820-020-0413-7

Chen, Z., Qin, Y., Amine, K., and Sun, Y. K. (2010). Role of surface coating on cathode materials for lithium-ion batteries. *J. Mater. Chem.* 20, 7606–7612. doi: 10.1039/C0JM00154F

Chi, Y.-W., Hu, C.-C., Shen, H.-H., and Huang, K.-P. (2016). New approach for high-voltage electrical double-layer capacitors using vertical graphene nanowalls with and without nitrogen doping. *Nano Lett.* 9, 5719–5727. doi: 10.1021/acs.nanolett.6b02401

Eftekhari, A. (2017). Supercapacitors utilising ionic liquids. *Energy Stor. Mater.* 9, 47–69. doi: 10.1016/j.ensm.2017.06.009

Elmouwahidi, A. E., Bailón-García, E., Castelo-Quibén, J., Perez-Cadenas, A., Maldonado Hodar, F. J., and Carrasco-Marin, F. (2017). Carbon-$TiO_2$ composites as high-performance supercapacitor electrodes: synergistic effect between carbon and metal oxide phases. *J. Mater. Chem. A.* 6, 1–3.

Gandla, D., Chen, H., and Tan, D. Q. (2020). High voltage and high energy supercapacitors based on biomass-derived hierarchical porous activated carbon. *Mater. Res. Express.* 7:08560. doi: 10.1088/2053-1591/abaf40

Gandla, D., and Tan, D. Q. (2019). Progress report on atomic layer deposition towards hybrid nanocomposite electrodes for next generation supercapacitors. *Adv. Mater. Interfaces.* 16:1900678. doi: 10.1002/admi.201900678

González, A., Goikolea, E., Barrena, J. A., and Mysyk, R. (2016). Review on supercapacitors: technologies and materials. *Renew. Sust. Energ. Rev.* 58, 1189–1206. doi: 10.1016/j.rser.2015.12.249

Ju, H., Liu, X. D., Tao, C. Y., Yang, F., and Zhang, L. (2020). Oxygen plasma functionalization of hexacyanocobaltates for high-capacity supercapacitor electrodes. *J. Electroanal. Chem.* 873:114382. doi: 10.1016/j.jelechem.2020.114382

Jung, Y. S., Lu, P., Cavanagh, A. S., Ban, C., Kim, G.-H., Lee, S.-H., et al. (2013). Unexpected improved performance of ALD coated $LiCoO_2$/graphite Li-ion batteries. *Adv. Energy Mater.* 3:213. doi: 10.1002/aenm.201200370

Kaus, M., Kowal, J., and Sauer, D. U. (2010). Modelling the effects of charge redistribution during self-discharge of supercapacitors. *Electrochimica Acta.* 55, 7516–7523. doi: 10.1016/j.electacta.2010.01.002

Kim, H. J., Yang, C. S., and Jeong, H. K. (2016). Electrochemical properties of modified highly ordered pyrolytic graphite by using ambient plasma. *Chem. Phys. Lett.* 644, 288–291. doi: 10.1016/j.cplett.2015.12.018

Korenblit, Y., Kajdos, A., West, W. C., Smart, M. C., Brandon, E. J., Kvit, A., et al. (2012). In situ studies of ion transport in microporous supercapacitor electrodes at ultralow temperatures. *Adv. Funct. Mater.* 8, 1655–1662. doi: 10.1002/adfm.201102573

Lai, C. C., and Lo, C. T. (2015). Plasma oxidation of electrospun carbon nanofibers as supercapacitor electrodes. *RSC Adv.* 5:38868. doi: 10.1039/c5ra04284d

Li, J.-Y., Song, X., Zhang, W.-M., Xu, H., Guo, T., Zhang, X., et al. (2020). Microporous carbon nanofibers derived from poly(acrylonitrile-co-acrylic acid) for high-performance supercapacitors. *Chem. Eur. J.* 26, 3326–3334. doi: 10.1002/chem.201904563

Li, J.-Y., Zhang, W.-M., Zhang, X., Huo, L.-Y., Liang, J.-Y., Wu, L.-S., et al. (2020). Copolymer derived micro/meso-porous carbon nanofibers with vacancy-type defects for high-performance supercapacitors. *J. Mater. Chem. A.* 8, 2463–2471. doi: 10.1039/C9TA08850D

Li, Z.-W., Bai, Z.-Y., Mi, H.-Y., Ji, C.-C., Gao, S., and Pang, H. (2019). Biowaste-derived porous carbon with tuned microstructure for high-energy quasi-solid-state supercapacitors. *Acs Sustain Chem Eng.* 15, 13127–13135. doi: 10.1021/acssuschemeng.9b02303

Liang, Z., Zhao, R., Qiu, T., Zou, R., and Xu, Q. (2019). Metal-organic framework-derived materials for electrochemical energy applications. *EnergyChem.* 1:100001. doi: 10.1016/j.enchem.2019.100001

Liu, D., Zhang, W., and Huang, W. (2019). Efect of removing silica in rice husk for the preparation of activated carbon for supercapacitor applications. *Chin. Chem. Lett.* 6, 1315–1319. doi: 10.1016/j.cclet.2019.02.031

Liu, M., Li, X., Karuturi, S. K., Tok, A. I. Y., and Fan, H. (2012). Atomic layer deposition for nanofabrication and interface engineering. *Nanoscale* 4, 1522–1528. doi: 10.1039/c2nr11875k

Morimoto, T., Hiratsuka, K., Sanada, Y., and Kurihara, K. (1996). Electric double-layer capacitor using organic electrolyte. *J. Power Sour.* 2, 239–247. doi: 10.1557/PROC-496-627

Murphy, A. B., Barnes, P. R. F., Randeniya, L. K., Plumb, I. C., Grey, I. E., Horne, M. D., et al. (2006). Effificiency of solar water splitting using semiconductor electrodes. *Int. J. Hydrogen Energy* 14, 1999–2017. doi: 10.1016/j.ijhydene.2006.01.014

Ouyang, B., Zhang, Y., Wang, Y., Zhang, Z., Fan, H. J., and Rawat, R. S. (2016). Plasma surface functionalization induces nanostructuring and nitrogen-doping in carbon cloth with enhanced energy storage performance. *J. Mater. Chem. A.* 4:17801. doi: 10.1039/c6ta08155j10.1039/c6ta08155j

Pandolfo, A. G., and Hollenkamp, A. F. (2006). Carbon properties and their role in supercapacitors. *J. Power Sour.* 1, 11–27. doi: 10.1016/j.jpowsour.2006.02.065

Qin, J., Sari, H. M. K., Wang, X., Yang, H., Zhang, J., and Li, X. (2020). Controlled design of metal oxide-based ($Mn^{2+}$/$Nb^{5+}$) anodes for superior sodium-ion hybrid supercapacitors: synergistic mechanisms of hybrid ion storage. *Nano Energy.* 71:104594. doi: 10.1016/j.nanoen.2020.104594

Shen, H.-H., and Hu, C.-C. (2014). Capacitance enhancement of activated carbon modified in the propylene carbonate electrolyte. *J. Electrochem. Soc.* 12, A1828–A1835. doi: 10.1149/2.0681412jes

Simon, P., and Gogotsi, Y. (2008). Materials for electrochemical capacitors. *Nat. Mater.* 7, 845–854. doi: 10.1038/nmat2297

Song, G. H., and Tan, D. Q. (2020). Atomic layer deposition for polypropylene film engineering-a review. *Macromol. Mater. Eng.* 2020:2000127. doi: 10.1002/mame.202000127

Sui, L., Tang, S., Chen, Y., Dai, Z., Huangfu, H., Zhu, Z., et al. (2015). An asymmetric supercapacitor with good electrochemical performances based on $Ni(OH)_2$/AC/CNT and ac. *Electrochim. Acta.* 182, 1159–1165. doi: 10.1016/j.elect

Surendran, S., Shanmugapriya, S., Shanmugam, S., Vasylechko, L., and Selvan, R. K. (2018). Interweaved nickel phosphide sponge as an electrode for flexible supercapattery and water splitting applications. *ACS Appl. Energy Mater.* 1, 78–92. doi: 10.1021/acsaem.7b00006

Tan, D. Q., Song, G., Gandla, D., and Zhang, F. (2020). Commonalities of atomic layer deposition of oxide coatings on activated carbons for 3.5V electric double layer supercapacitors. *Front. Energy Res.* 8:596062. doi: 10.3389/fenrg.2020.596062

Tao, L., Wang, Q., Dou, S., Ma, Z., Huo, J., Wang, S., et al. (2016). Edge-rich and dopant-free graphene as a highly efficient metal-free electrocatalyst for the oxygen reduction reaction. *Chem. Commun.* 52:2764. doi: 10.1039/C5CC09173J

Tran, M. H., Yang, C. S., and Jeong, H. K. (2016). Fast and economical reduction of poly (sodium 4-styrene sulfonate) graphite oxide film by plasma. *Electrochimica Acta.* 196, 769–774. doi: 10.1016/j.electacta.2016.03.004

Wang, F., Xiao, S., Hou, Y., Hu, C., Liu, L., and Wu, Y. (2013). Electrode materials for aqueous asymmetric supercapacitors. *RSC Adv.* 32, 13059–13084.

Wang, K.-B., Xun, Q., and Zhang, Q. (2020). Recent progress in metal-organic frameworks as active materials for supercapacitors. *Energy Chem.* 2:100025. doi: 10.1016/j.enchem.2019.100025

Wang, Y., Wang, X., Li, X., Li, X., Liu, Y., Bai, Y., et al. (2020). A high performance, tailorable, wearable, and foldable solid state supercapacitor enabled by arranging pseudocapacitive groups and MXene flakes on textile electrode surface. *Adv. Funct. Mater.* 31:2008185. doi: 10.1002/adfm.202008185

Xue, D., Zhu, D., Liu, M., Duan, H., Li, L., Chai, X., et al. (2018). Schiff-base/resin copolymer under hypersaline condition to high-level n doped porous carbon nanosheets for supercapacitors. *ACS Appl. Nano Mater.* 1, 4998–5007. doi: 10.1021/acsanm.8b01125

Yan, J., Fang, Y. Y., Wang, S. W., Wu, S. D., and Liu, F. J. (2020). Nitrogen-doped oxygen-rich activated carbon derived from Longan shell for supercapacitors. *Int J. Electrochem. Sci.* 15, 1982–1995. doi: 10.20964/2020.03.18

Yan, J., Wang, Q., Wei, T., and Fan, Z. (2013). Recent advances in design and fabrication of electrochemical supercapacitors with high energy densities. *Adv. Energy Mater.* 4:1300816. doi: 10.1002/aenm.201470017

Yoshida, A., Tanahashi, I., and Nishino, A. (1990). Effect of concentration of surface acidic functional groups on electric double-layer properties of activated carbon fibers. *Carbon* 5, 611–615. doi: 10.1016/0008-6223(90)90062-4

Zeng, L., Lou, X., Zhang, J., Wu, C., Liu, J., and Jia, C. (2019). Carbonaceous mudstone and lignin-derived activated carbon and its application for

supercapacitor electrode. *Surf. Coat. Technol.* 357, 580–586. doi: 10.1016/j.surfcoat.2018.10.041

Zhang, Y., Rawat, R. S., and Fan, H. J. (2017). Plasma for rapid conversion reactions and surface modification of electrode materials. *Small Methods* 1:1700164. doi: 10.1002/smtd.201700164

Zhao, J. Q., and Wang, Y. (2012). Ultrathin surface coatings for improved electrochemical performance of lithium ion battery electrodes at elevated temperature. *J. Phys. Chem. C.* 116, 11867–11876. doi: 10.1021/jp3010629

Zhao, J. Q., and Wang, Y. (2013). Surface modifications of Li-ion battery electrodes with various ultrathin amphoteric oxide coatings for enhanced cycleability. *J. Solid State Electrochem.* 17, 1049–1058. doi: 10.1007/s10008-012-1962-6

Zhou, Q., Zhao, Z., Chen, Y., Hu, H., and Qiu, J. (2012). Low temperature plasma-mediated synthesis of graphene nanosheets for supercapacitor electrodes. *J. Mater. Chem.* 13:6061. doi: 10.1039/C2JM15572A

**Conflict of Interest:** The authors declare that the research was conducted in the absence of any commercial or financial relationships that could be construed as a potential conflict of interest.